Paper Number: 281

# Title: A numerical and experimental study of damage growth in a composite laminate

Authors: Mark McElroy[1], James Ratcliffe[2], Michael Czabaj[2], John Wang[2], Fuh-Gwo Yuan[1,3*]

**SUMMARY**

The present study has three goals: (1) perform an experiment where a simple laminate damage process can be characterized in high detail; (2) evaluate the performance of existing commercially available laminate damage simulation tools by modeling the experiment; (3) observe and understand the underlying physics of damage in a composite honeycomb sandwich structure subjected to low-velocity impact. A quasi-static indentation experiment has been devised to provide detailed information about a simple mixed-mode damage growth process. The test specimens consist of an aluminum honeycomb core with a cross-ply laminate facesheet supported on a stiff uniform surface. When the sample is subjected to an indentation load, the honeycomb core provides support to the facesheet resulting in a gradual and stable damage growth process in the skin. This enables real time observation as a matrix crack forms, propagates through a ply, and then causes a delamination. Finite element analyses were conducted in ABAQUS/Explicit® 6.13 that used continuum and cohesive modeling techniques to simulate facesheet damage and a geometric and material nonlinear model to simulate core crushing. The high fidelity of the experimental data allows a detailed investigation and discussion of the accuracy of each numerical modeling approach.

---

[1]Department of Mechanical and Aerospace Engineering,
North Carolina State University, Raleigh, NC 27695
[2]NASA Langley Research Center, Hampton, VA, 23666
[3]National Institute of Aerospace, Hampton, VA, 23666
*Corresponding Author: mwmcelro@ncsu.edu

## 1. INTRODUCTION

The development of predictive capabilities for modeling progressive damage in fiber-reinforced polymer (FRP) composite laminates over the past several decades has resulted in a number of techniques as summarized in [1]. Particular focus has been given to the simulation of delamination due to its importance to damage resistance and tolerance of FRP laminates. Two main techniques, namely cohesive zone modeling [2] and the virtual crack closure technique (VCCT) [3,4], have been developed and implemented into the finite element analysis (FEA) framework to model delamination. The former method uses a traction separation law while the latter is based on Irwin's crack closure integral [5]. More recently, simulation of intralaminar damage in the form of matrix cracks has been made possible by techniques such as the extended finite element method (XFEM) [6] and continuum damage mechanics [7]. Many variations and combinations of these numerical techniques have been studied and implemented to varying levels of success.

Several modes of damage can occur in FRP composite laminates. These include largely fiber failure, matrix cracks, and delaminations. As failure and deformation occur, these separate damage processes may take place simultaneously and can significantly influence each other. While the numerical tools mentioned above may be capable of simulating each of the isolated damage processes well, it is simulating the interaction of these processes that can be challenging in composite laminate damage growth modeling. For instance, simulation methods successfully applied to analysis of open-hole tension specimens [8] did not perform as well when applied to delamination in non-unidirectional double cantilever beam specimens [9]. The clear need for greater understanding of damage mode interaction has therefore yielded a number of recent experimental and analytical studies [10, 11, and 12].

One drawback of using composite laminates for aerospace structures is their susceptibility to damage when subjected to a transverse load. A load of this nature often is in the form of low-velocity impact and can result in what is commonly referred to as barely visible impact damage (BVID). Compressive strength of FRP laminates can be significantly reduced if this occurs and can thus act as a major driver in the sizing of composite structures [13]. A typical interaction of damage processes resulting from low-velocity impact takes the form of an evolving network of interconnected matrix cracks and delamination. The crack network can grow in three dimensions from a single initiation point until all external work on the structure has been dissipated through strain energy release, material damage, and damping. A simple example of this type of damage pattern is shown in Figure 1 [14]. This damage process, shown here in its final state, consists of delaminations that have migrated to multiple plies via matrix cracks.

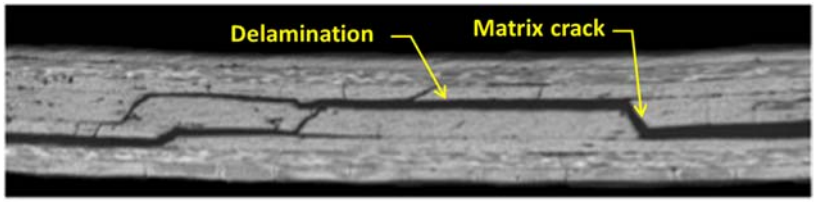


Figure 1. Typical laminate damage pattern.

It is possible that a different and specifically designed numerical tool can be used for each type of damage mode occurring within a single finite element model. If this is the case, then as discussed, their independent accuracy and their ability to interact are equally important. The commercial finite element analysis software ABAQUS/Explicit® 6.13 [15] has all of the damage simulation techniques mentioned above implemented. They all are theoretically capable of being utilized and combined with one another to simulate complex composite laminate damage processes. The goal of this study is to conduct an experiment where a simple laminate damage process in a composite honeycomb facesheet can be observed in detail and then investigate the capabilities of existing numerical tools in ABAQUS/Explicit® 6.13 as a means to perform an equivalent simulation.

A challenge in understanding low-velocity impact damage processes in composite laminates is that they occur very quickly and often only the final permanent damage state can be characterized in detail. Intermittent states of damage during the load duration are of great interest in developing a damage simulation tool. Quasi-static indentation has been shown to result in structural and material behavior that is equivalent to that of a low-velocity impact load [16, 17, and 18]. This equivalency is based on the requirement that a structure does not have an appreciable dynamic response to a low-velocity impact load. In this case, the deformation is the same as it would be if the load were static (or of much longer duration). The term “low-velocity impact” is loosely defined but in general implies loading and structural (i.e., mass and stiffness) conditions that meet this criterion. The present study consists of quasi-static indentation testing on sandwich panels, and because of this equivalence in behavior, is applicable to low-velocity impact damage.

## 2. EXPERIMENTATION

### 2.1 Test Specimen Description

The test specimen is illustrated in Figure 2. It consists of an aluminum honeycomb core sandwiched between two carbon fiber-reinforced polymer (CFRP) facesheets. The specimens are placed on a rigid base and indented quasi-statically. In each specimen, the top facesheet contains a Teflon insert that serves as a preexisting delamination of length $a_0$. The Teflon inserts, located centrally relative to the specimen span, are placed below the upper $0^0$ stack that contacts the indenter and above a $90^0$ stack. This arrangement results in a damage process that consists of the following: (1) an intralaminar matrix crack initiates at the end of the preexisting delamination and grows down through the $90^0$ stack, (2) the matrix crack is arrested at the lower surface of the $90^0$ stack when it reaches a ply of differing fiber orientation, and (3) the crack turns and takes the form of a delamination that propagates away from the indenter. This process is illustrated in Figure 2 (see dotted blue line) and similar to that shown in Figure 1 where a delamination migrates though a stack of plies via a matrix crack and then continues along a new laminate interface.

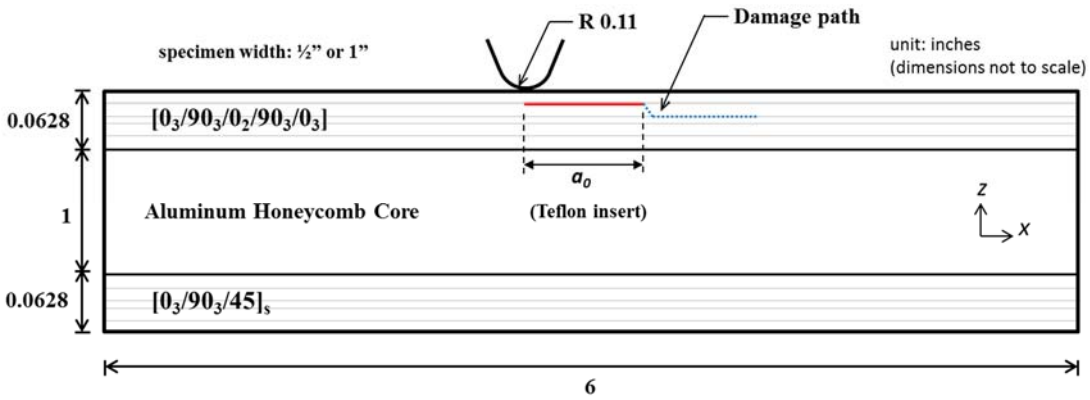


Figure 2. Test specimen geometry and layup.

The sandwich core material in this experiment is specifically included as a means to stabilize the damage process in the facesheet. The core, acting as a deformable foundation, provides support limiting facesheet deflection at locations away from the indenter. The support from the core results in a localized deformed state where most of the energy from external work is absorbed, not by global facesheet deflection (as would occur if the core was not present) but by honeycomb crushing in the vicinity of the indenter. Thus the amount of stored strain energy in the specimen is limited and as a result, when an initial flaw is included, the damage in the facesheet is a gradual stable process that can be well characterized in real time.

## 2.2 Materials and Specimen Manufacture

A 12"×12" composite sandwich panel consisting of two IM7/8552 laminate facesheets and an aluminum honeycomb core (Hexcel type: CR III–3/16–5052–.0015N–4.4) was fabricated. Facesheets were first laid up in accordance with the stacking sequences shown in Figure 2. Although the panels are asymmetric due to the differing facesheets, no measureable panel warp was seen after manufacture. Teflon insert strips, 0.0005" thick and varying in length, $a_0$, between ¼" and ½", were implanted in several quadrants of the facesheets at the interface indicated in Figure 2. The facesheets were cured in a hot press using a cycle recommended by the material manufacturer. The cured facesheets and core were co-bonded using AF-555 film adhesive in a hot press using the adhesive manufacture's recommended cure cycle. A total of twenty-four 6" long specimens were cut from the panel in widths of both ½" and 1" such that a Teflon insert is present in one facesheet only.

## 2.3 Test Procedure

Quasi-static indentation tests were performed using a servo hydraulic test stand equipped with a 2900 lb load cell. Specimens were positioned on a rigid base and indented with a 0.11 in-radius tip indenter under displacement control at a rate of 0.005 in/min. Tests were performed for specimens both with and without a Teflon insert present in the loaded facesheet. In cases where the loaded facesheet

contained a Teflon insert, the indenter was aligned with one of the Teflon insert fronts as illustrated in Figure 2. Specimens with pristine facesheets were indented along their mid span. Specimens were unloaded at a rate of 0.01 in/min after a desired amount of damage had occurred. In some instances, specimens were subjected to several loading cycles involving an increased amount of maximum indentation for each successive cycle. In these tests, specimens were C-scanned after each loading cycle. Indenter force displacement response was recorded throughout the test using a sample rate of 0.5 Hz. The edges of the indented facesheets were painted white with diluted liquid correction fluid to highlight edge-view delamination and crack migration during a test. Initiation and progression of these events was documented using two digital cameras equipped with macro lenses positioned on each side of a specimen. A picture of a typical test configuration is shown in Figure 3. One test was performed where a digital image correlation system [19] was utilized to measure vertical facesheet deformation of a specimen with a pristine loaded facesheet.

## 3. ANALYSIS

Simulations of the indentation tests were performed using the commercial finite element analysis software ABAQUS/Explicit® 6.13. The goal of these analyses was to evaluate the current capability of numerical tools in ABAQUS/Explicit® 6.13. Three different simulations were run. The first was of an indented specimen with a pristine facesheet. The second and third simulations contained the embedded delamination in the loaded facesheet. These two models used cohesive zones and continuum damage mechanics respectively to simulate facesheet damage. All three models contained a high fidelity mesh in the honeycomb cells and used material and structure damage models to simulate core crushing. For the remainder of the paper, the focus is on one test specimen with the following configuration: width = ½ in, delamination length $a_0$ = ½ in (or $a_0$=0 in for the case of the pristine specimen), indented facesheet layup = $[0_3/90_3/0]_s$. The maximum indenter displacement is 0.041 in.

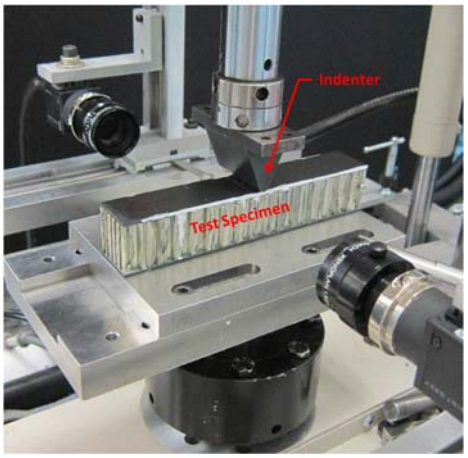


Figure 3. Test configuration of a composite honeycomb specimen under quasi-static indentation.

### 3.1 Finite Element Model Overview

A generic finite element model is depicted in Figures 4a – 4c. Material and strength properties for the composite facesheet material (IM7/8552) and aluminum honeycomb core are shown in Tables Ia [20] and Ib [21], respectively. The honeycomb core is modeled explicitly using S4R shell elements. The meshes and element types used to model the upper facesheet (in contact with the indenter) varies among models and will be described in the following sections. The top of the core mesh is coincident with the mesh in the lowest ply of the top facesheet and attached via a shell-to-solid constraint. There is a tie constraint [15] between the top of the lowest stack and the rest of the facesheet.

The lower facesheet is modeled with a mesh composed of composite S4R elements that is merged with the bottom of the core mesh. The whole specimen is placed on an analytical rigid surface that is fixed. The indenter consists of an analytical rigid surface that has a vertical displacement defined as a boundary condition. A general contact definition is defined in the model to capture contact between the indenter and the upper facesheet, contact between the rigid base surface and the lower facesheet, and contact of honeycomb cell walls with each other during core crushing.

The rigid base and associated contact is effectively a boundary condition in the vertical direction where the specimen can lift off and deflect upwards but not downwards. Additional boundary conditions were defined on two edges of the bottom facesheet as shown in Figure 4c.

While the upper facesheet mesh, element type, and damage technique varied between simulations, the honeycomb mesh and damage simulation is the same in all of the models. Damage in the core during the crushing process consists of both structural and material failure. Structural failure is in the form of buckling and is captured by enabling geometrically nonlinear behavior in the analysis solution. Material failure occurs in the form of yielding of the honeycomb cell walls and was simulated by defining a nonlinear plasticity model. Material data are unavailable for the core material aluminum alloy 5052-H39, so properties for 5052-H38 were obtained and used instead. The nonlinear stress-strain relation used in the plasticity model is shown in Figure 5 and is defined using the values in Table Ib for yield and plastic stress-strain data points (i.e. $\sigma_y$, $\sigma_{pl}$, $\varepsilon_{pl}$). The core model initially was discovered to be too stiff in its crushed state, so the final two points in the plastic stress-strain curve, defined in ($x$,$y$) coordinates by ($\sigma_{pl,3}$, $\varepsilon_{pl,3}$) and ($\sigma_{pl,4}$, $\varepsilon_{pl,4}$), were added to simulate a level of increased failure/damage occurring after ultimate stress is reached. The plasticity model can therefore be thought of as an enhanced model as its simulation capability extends beyond ultimate stress.

All analyses were run using ABAQUS/Explicit® 6.13. The vertical displacement of the indenter was applied in a dynamic step lasting 2 seconds. Because mass scaling was defined to enable a timely solution, it was verified that for all analyses performed, the kinetic energy was negligible compared to external work and internal strain energy. Additionally, the applied and reaction forces were compared to ensure that they matched indicating there was no appreciable inertial force present in the simulation. These checks were made to verify that unrealistic dynamic behavior was not present and that the simulations were truly quasi-static in nature.

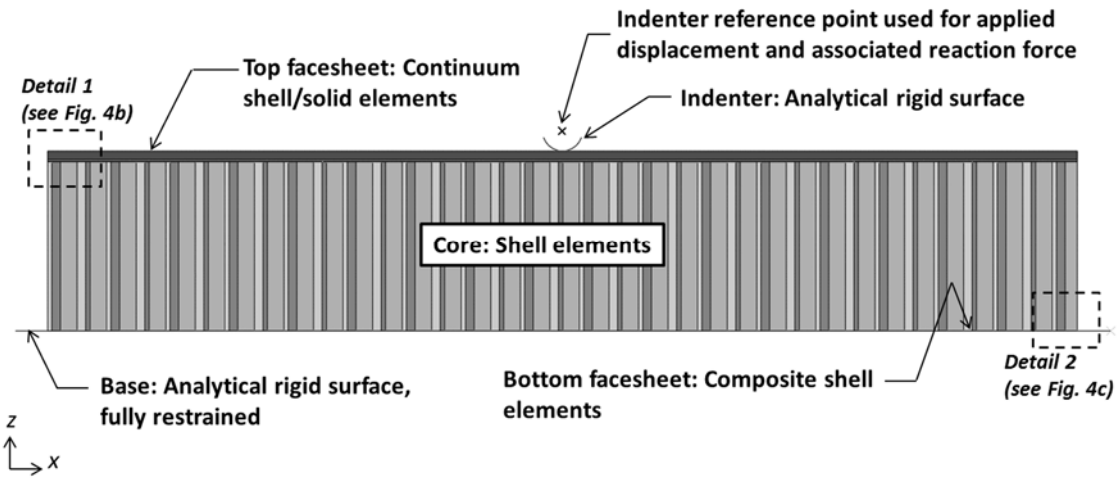


a. Finite element model.

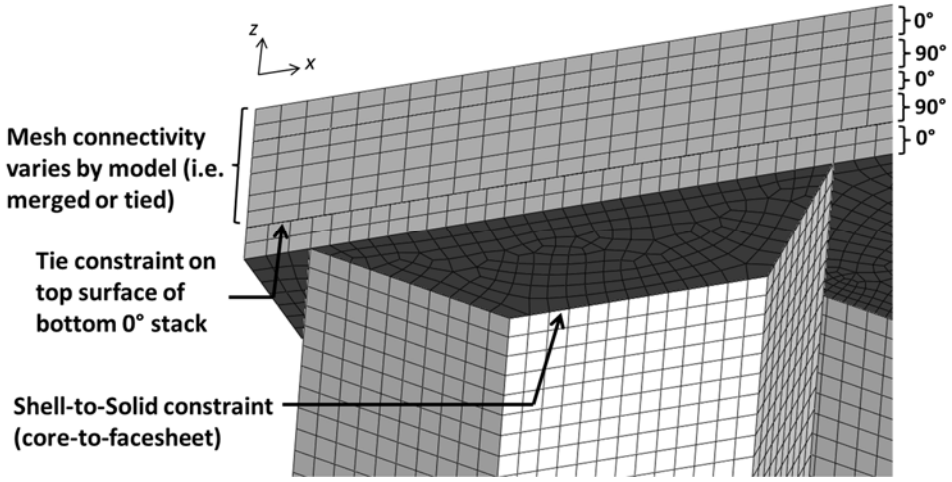


b. Detail 1.

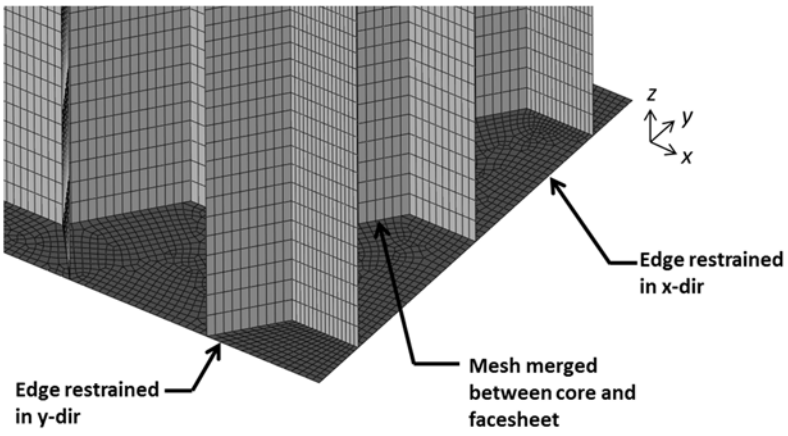


c. Detail 2.

Figure 4. Finite element model overview.

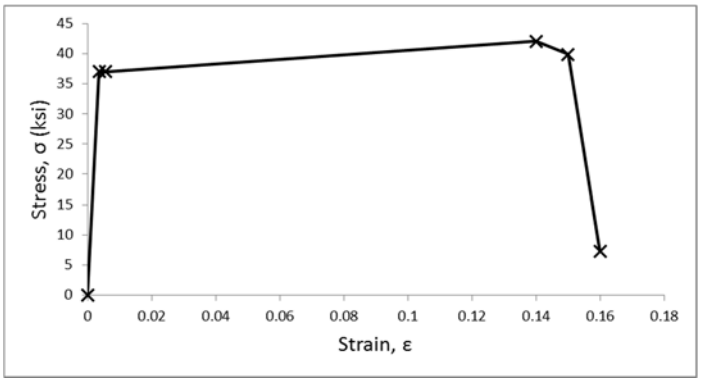


Figure 5. Enhanced Al 5052-H38 plasticity model.

Mesh convergence studies were performed for the loaded facesheet and the core meshes. The converged facesheet mesh and element type varied among models and will be discussed in detail in the following sections. The exception to this is the mesh in the bottom zero degree stack. Since the bottom ply mesh is coincident with the top of the core mesh, which is the same for all models, the mesh in this stack is also the same for all models. There are two elements through the thickness of the bottom stack. An element size of 0.0078 in was used in the core mesh for all models.

### 3.2 Pristine Facesheet Model (PFM)

The first simulation performed corresponds to the test where no Teflon insert was present in the loaded facesheet. In this test, the damage behavior can be seen to be entirely composed of core crushing. This simulation was performed first to validate the model behavior before considering the additional complexity of a facesheet damage process. The upper facesheet in this model was composed of C3D8R solid elements sized at approximately 0.015 in. Aside from the bottom stack, there is one element in the thickness direction per stack.

### 3.3 Cohesive Zone Model (CZM)

In the CZM, the damage path was entirely prescribed in the facesheet as a cohesive zone as shown in Figure 2. The cohesive zone was implemented in the model as a cohesive surface using the parameters shown in Table Ia. In cohesive damage models, a nonlinear traction law as shown in Figure 6 is defined between two node surfaces in a mesh. The cohesive law contains an initial undamaged elastic behavior regime where the surfaces are effectively attached to one another. A damage initiation stress threshold is defined that initiates a softening behavior regime where a degradation of stiffness that increases as the surfaces move away from one another occurs. Eventually, the two surfaces achieve a level of separation such that the stiffness connecting them is zero and they are completely “unattached” from one another [2].

For damage initiation, a quadratic traction criterion was used to allow for mode mixity and is defined in Equation 1. The subscripts on the traction terms, *t*,

indicate normal (*n*), first shear (*s*), and second shear (*t*) components. The terms in the denominators refer to the damage initiation stress thresholds for their associated stress component. These terms are included in Table Ia and listed as $Y^T$ and $S^{12}$.

$$\left\{\frac{\langle t_n \rangle}{t_n^o}\right\}^2 + \left\{\frac{t_s}{t_s^o}\right\}^2 + \left\{\frac{t_t}{t_t^o}\right\}^2 = 1 \qquad (1)$$

As the surfaces separate and damage evolves, mode mixity is captured using linear softening in an energy based Benzeggagh-Kenane law [22]. A convergence study was conducted to verify that use of a viscous stabilization coefficient of 2 x $10^{-4}$ would improve solution convergence but not sacrifice accuracy. The top facesheet mesh is composed of C3D8R solid elements sized at approximately 0.0098 in with two elements through the thickness of each stack.

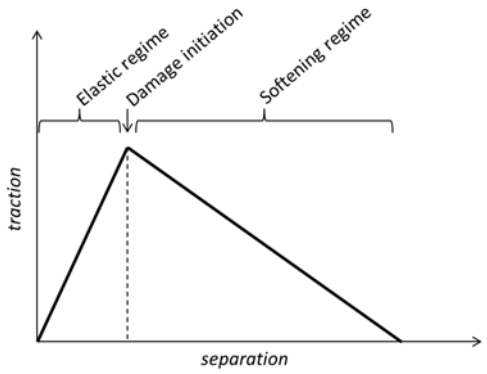


Figure 6. Cohesive traction separation law.

TABLE Ia. IM7/8552 MATERIAL & STRENGTH PROPERTIES [20]

| **Parameter** | **Value** | **Units** |
|---|---|---|
| $E_{11}$ | 24.85 (171.4) | ksi (MPa) |
| $E_{22}$ | 1.32 (9.08) | ksi (MPa) |
| $E_{33}$ | 1.32 (9.08) | ksi (MPa) |
| $G_{12}$ | 0.77 (5.29) | ksi (MPa) |
| $G_{13}$ | 0.77 (5.29) | ksi (MPa) |
| $G_{23}$ | 0.41 (2.8) | ksi (MPa) |
| $\nu_{12}$ | 0.32 | - |
| $\nu_{13}$ | 0.32 | - |
| $\nu_{23}$ | 0.5 | - |
| | | |
| $X^T$ | 337.30 (2326.2) | ksi (MPa) |
| $X^C$ | 174.01 (1200.1) | ksi (MPa) |
| $Y^T$ | 9.03 (62.3) | ksi (MPa) |
| $Y^C$ | 28.97 (199.8) | ksi (MPa) |
| $S^{12}$ | 13.38 (92.3) | ksi (MPa) |
| | | |
| $G_{Ic}$ | 0.13 (0.277) | ft-lb/in$^2$ (kJ/m$^2$) |
| $G_{IIc}$ | 0.37 (0.788) | ft-lb/in$^2$ (kJ/m$^2$) |
| $\eta_{BK}$ | 1.634 | - |
| | | |
| $\rho$ | 0.0567 (1.55) | lb/in$^3$ (g/cm$^3$) |

TABLE Ib. ALUMINUM ALLOY 5052-H38 MATERIAL PROPERTIES [21]

| Parameter | Value | Units |
|---|---|---|
| $E$ | 10194 (70300) | ksi (MPa) |
| $\nu$ | 0.33 | - |
| $\rho$ | 0.097 (2.69) | lb/in$^3$ (g/cm$^3$) |
| $\sigma_y$ | 36.98 (255) | ksi (MPa) |
| $\varepsilon_y$ | 0.0036 | - |
| $\sigma_{pl,1}$ | 36.98 (255) | ksi (MPa) |
| $\sigma_{pl,2}$ | 42.05 (290) | ksi (MPa) |
| $\sigma_{pl,3}$ | 39.88 (275) | ksi (MPa) |
| $\sigma_{pl,4}$ | 7.25 (50) | ksi (MPa) |
| $\varepsilon_{pl,1}$ | 0.0056 | - |
| $\varepsilon_{pl,2}$ | 0.14 | - |
| $\varepsilon_{pl,3}$ | 0.15 | - |
| $\varepsilon_{pl,4}$ | 0.16 | - |

### 3.4 Continuum Damage Model (CDM)

The CDM uses the Hashin damage initiation criteria and its associated stiffness degradation model as it is implemented in ABAQUS/Explicit® 6.13 [15] for facesheet elements in the vicinity of the matrix crack. The Hashin criteria can be found in references [15, 23]. Element stiffness degradation is achieved by including matrix and fiber damage terms, $d_m$ and $d_f$, respectively, in the element stiffness matrix, $C$, as shown in Equations (2a) and (2b). Damage evolution occurs according to a stress displacement relation and is such that the terms $d_m$ and $d_f$ increase as damage increases. The delamination path is prescribed as a cohesive surface that extends in both directions from the matrix crack location (this is different than the CZM where the delamination was prescribed only in the direction seen in testing). The Hashin/continuum damage mechanics model is implemented in ABAQUS/Explicit® 6.13 for planar type elements only, so the upper facesheet was composed of SC8R continuum shell elements sized at approximately 0.0098 in. All stacks have two elements through the thickness except for the stack where the migration occurs. This stack has three elements through the thickness.

$$C = \frac{1}{D}\begin{bmatrix} (1-d_f)E_1 & (1-d_f)(1-d_m)\nu_{12}E_1 & 0 \\ (1-d_f)(1-d_m)\nu_{12}E_1 & (1-d_m)E_2 & 0 \\ 0 & 0 & (1-d_s)GD \end{bmatrix} \quad (2a)$$

$$D = 1-(1-d_f)(1-d_m)\nu_{12}\nu_{21} \quad (2b)$$

## 4. RESULTS AND DISCUSSION

### 4.1 Pristine Facesheet Model (PFM)

The first tests performed were on specimens that did not contain a Teflon insert in the loaded facesheet. A deformed plot of the corresponding model shown in Figure 7 serves as validation that the honeycomb cells are generally deforming and buckling in the same manner as seen in testing. A more precise validation of the model is achieved by comparing the deformed shape of the loaded facesheet along one edge in the model with that of the test where digital image correlation data were gathered. This validation is shown in Figure 8. Force displacement data collected at the indenter are compared to analysis results and are shown in Figure 9.

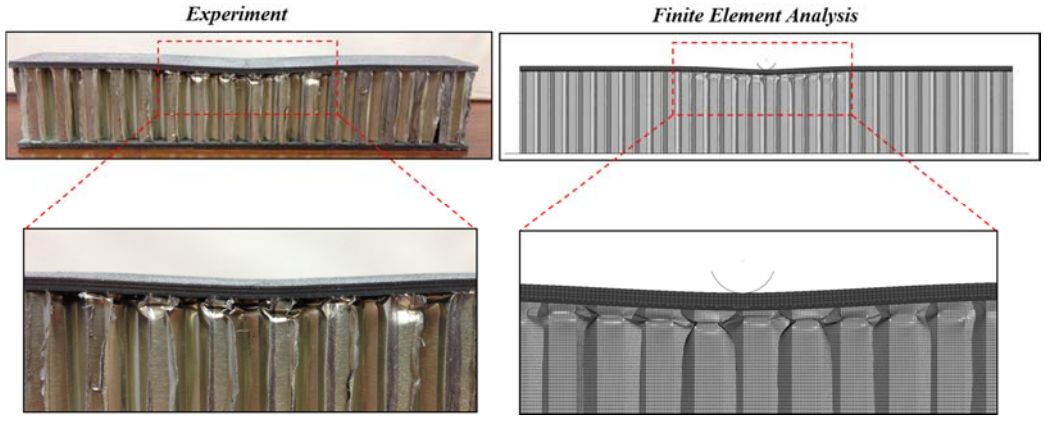


Figure 7. PFM: comparison of honeycomb core deformation between experiment and finite element analysis (no initial delamination present).

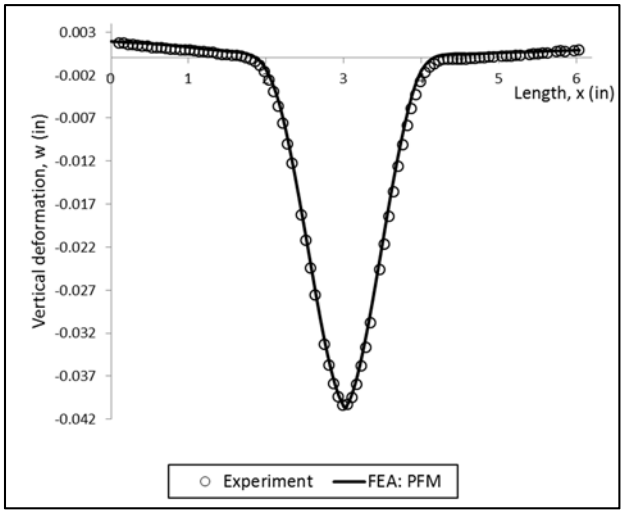


Figure 8. PFM: facesheet deformation data correlation.

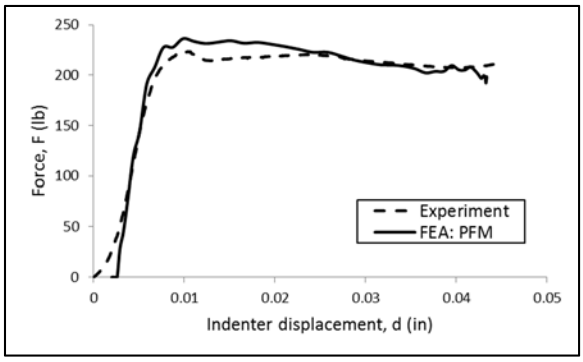


Figure 9. PFM: force displacement data correlation.

The comparisons in Figures 7-9 all indicate that the finite element model is capable of simulating the core crush and associated facesheet deformation behavior for cases where there is no damage process occurring in the facesheet. Particularly encouraging is the close agreement in the facesheet deformed shape seen in Figure 8. Therefore, the stress state of the facesheet is well captured by the model at all points along its length, not just where the load is applied.

### 4.2 Cohesive Zone Model (CZM)

The cohesive zone based simulation uses a prescribed damage path to predefine the location of the migration and delamination. In taking this approach, the damage process is essentially forced to propagate correctly. This model, therefore, is somewhat contrived to achieve an accurate result though it still is useful in two main ways. The first is that it can show whether or not the model as a whole is valid *if* the facesheet damage model is accurate. If this is demonstrated, alternate more general facesheet damage models with enhanced predictive capabilities can be investigated. The second use for this model is to evaluate the accuracy of a cohesive zone in simulating delamination cracks. The requirement for cohesive models to have a predefined crack path is not necessarily a limitation when it comes to delamination. The location of delaminations is always known to be in between plies. Ply interfaces in a finite element mesh can be convenient places to insert a predefined delamination path.

Figure 10 shows the final damaged state of the facesheet in the model compared to an experimentally obtained image. Figure 11 contains experimental force displacement plots from two specimens. The first dramatic change in slope of the curves is due to the sudden buckling of honeycomb cells in the vicinity of the indenter. The intralaminar crack formation and subsequent delamination growth is indicated on each curve.

When compared to the curve in Figure 9 for the case where there are no facesheet cracks, it is evident that the specimens with a Teflon insert have a lower strength due to the presence of the embedded crack, but that the curves still retain a similar shape. It appears that at the start of the delamination in Figure 11, the curves change to a negative slope. This makes sense as it indicates a continuing reduction in stiffness caused by the delamination growth.

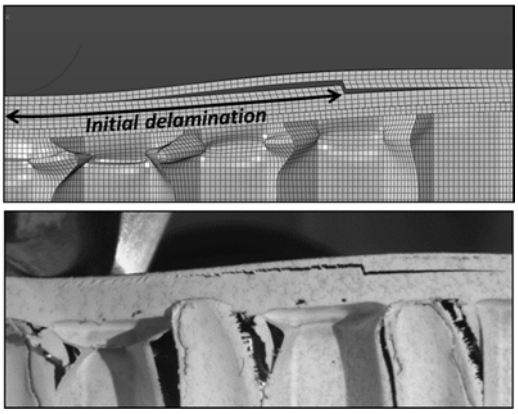


Figure 10. CZM: visual data correlation of facesheet damage.

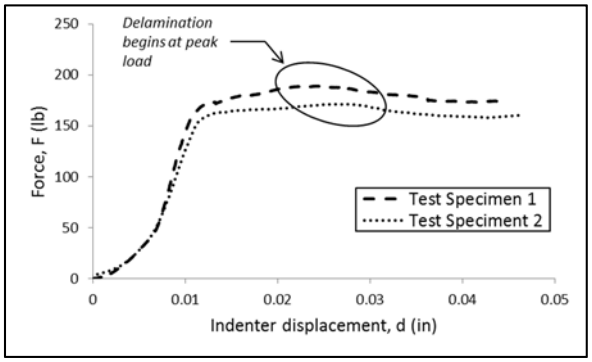


Figure 11. Experimental force displacement relation with initial delamination present.

An interesting observation is that the point where the force displacement curve flattens out in Figure 11 does not correspond with initiation of facesheet cracking. The specimen indentation response is dominated by the core crushing. Facesheet damage as an energy dissipation mechanism is small compared to core crushing and almost indiscernible on the force displacement plot. A result of this is the slow stable facesheet damage growth that is desired for this test.

A good correlation of force displacement data between the model and the test is shown in Figure 12. Deserving some explanation is the initial nonlinear portion of the experimental curve in Figures 11 and 12. An investigation was performed on one of the specimens to determine the cause of this initial nonlinear behavior. It was found that a very small rotation was occurring in the specimen at the beginning of the test. Measurements from calibrated photos indicate that one side of the facesheet was deforming faster than the other for a short period at the beginning of the test. The magnitude of this difference in deformation rate for each side corresponds with the nonlinear portion of the force displacement curve. This correlation is shown in Figure 13. The percent difference in deflection rate for each side of the specimen approaches zero as the force displacement becomes linear. This indicates that the sample may have been initially warped and “settled” slightly before establishing uniform contact with the base and indenter. An indentation test

was also performed on an aluminum block and it was determined from this test that there is very little nonlinearity due to the compliance of the test stand.

The finite element models do not experience any of this initial "settling" behavior since they represent an ideal case. Therefore, to properly correlate the numerical and experimental data, the finite element force displacement curves are always offset along the displacement axis such that the linear portions of the force displacement curve align with one another. This represents a theoretical case where there is no nonlinearity in the experiment.

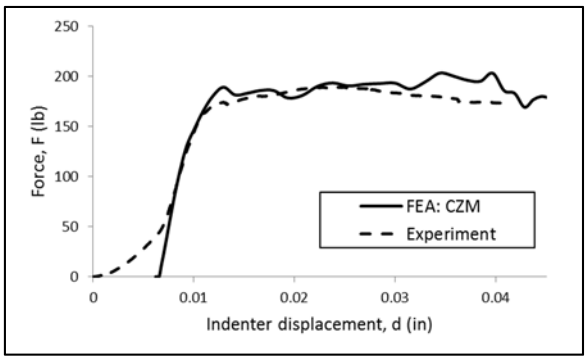


Figure 12. CZM: force displacement data correlation.

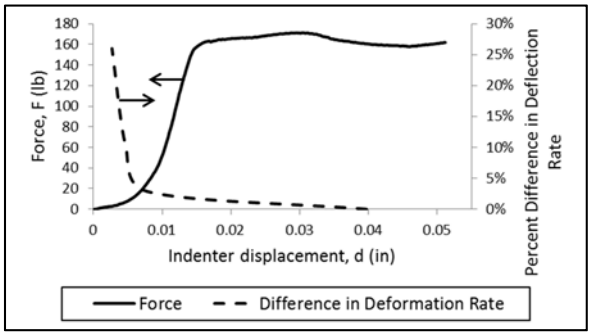


Figure 13. Nonlinear force displacement correlation with specimen "settling".

Figure 14 is a plot of delamination length versus indenter displacement. In Figure 14, the FEA and Specimen 1 curves are both offset along the horizontal axis by the amount that aligns the linear portion of their respective force displacement curves with that of Specimen 2. The model predicts well the initiation point of the delamination at an indentation displacement of approximately 0.02 in. The simulation tends to underpredict crack length through most of the growth process, however, a fairly close match is seen with Specimen 2. The final crack length matches well falling within 8% of the average of the maximum crack length from the two data sets. A comparison of the delamination is shown in plan view in Figure 15 where a cohesive damage contour plot from the model and a C-scan of specimen 2 after indentation are shown side by side. The model predicts well the "toenail" shaped crack front through the width of the specimen.

An important feature of the model has to do with the presence of multiple simultaneous damage modes. Core crushing and crack propagation can be seen as two independent damage processes with independent damage models, however, at the same time, they influence one another. The CZM was shown to capture this complex interaction accurately and provides a base level of confidence that builds on the results from PFM. In Section 4.1, it was determined that the core damage model was accurate when it was the only damage process occurring. Data from this section demonstrate that (1) *if* the facesheet damage model is accurate, the simulation as a whole is accurate and (2) the cohesive damage modeling technique for delamination cracks can be accurate. This sets the stage for investigation of other damage modeling techniques in the facesheet that may provide a higher level of predictive capability.

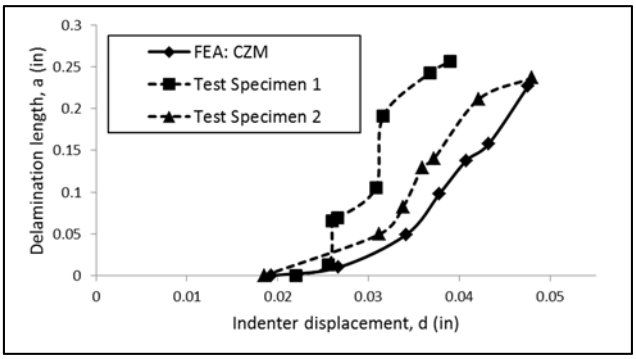


Figure 14. CZM: delamination length data correlation.

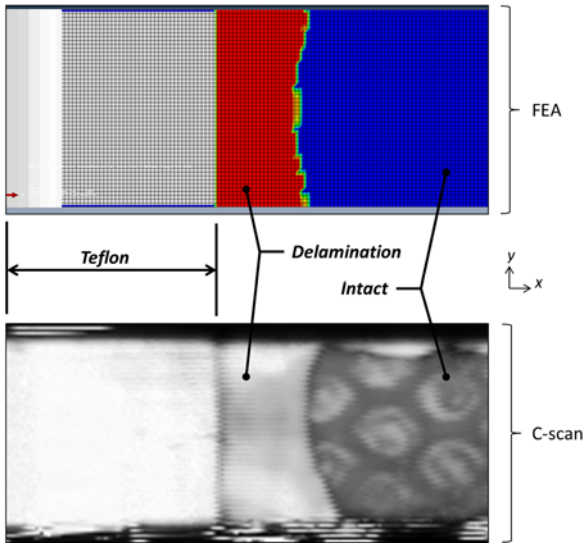


Figure 15. CZM: delamination front data correlation (plan view of specimen).

### 4.3 Continuum Damage Model (CDM)

The second facesheet damage modeling approach investigated was continuum damage mechanics. The intent of this model was to run a simulation where the migration location was not predefined. This is a marked improvement in predictive capability when compared to the cohesive damage model. Key features to capture in this model are the initiation and location of the migration as well as the turning of this matrix crack into a delamination. Figure 16 shows the final damaged state of the model compared to an experimentally obtained image. The deformation of the damaged facesheet is not as dramatic as seen in the purely cohesive model. To highlight better the damage that has occurred in the simulation, Figure 17 shows contour plots of Hashin matrix tension failure criteria, representing the matrix crack, and cohesive damage, representing delamination.

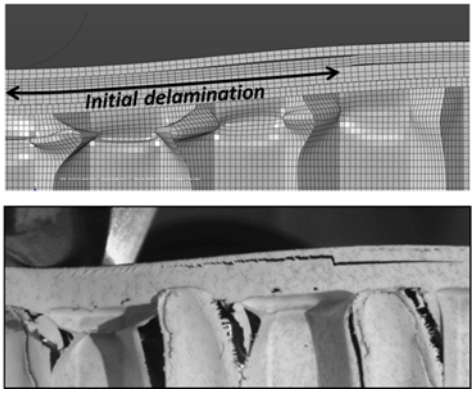


Figure 16. CDM: visual data correlation of facesheet damage.

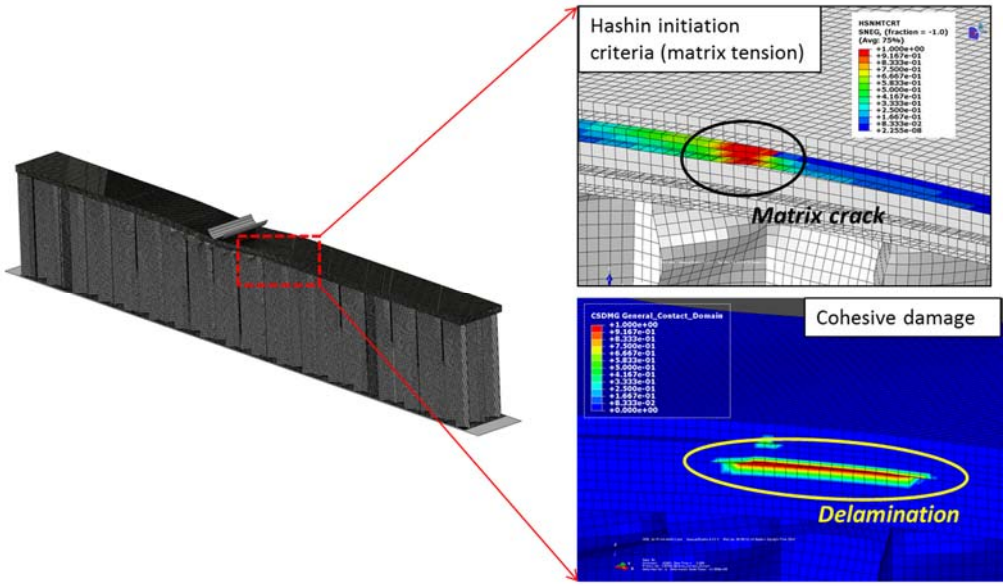


Figure 17. CDM: facesheet damage contour plots.

Figure 18 shows the indenter force displacement data from the model and testing. The force displacement data show a good match with the experimental data. The model curve is offset as before to align with the elastic portion of the experimental curve. Figure 19 contains a plot of delamination length versus indenter displacement. The facesheet damage process is simulated correctly in terms of crack type and sequence of events, but the growth of the delamination does not match well with data from digital images of the facesheet edge. The delamination is shown in plan view in Figure 20 as a cohesive damage contour plot and compared to a C-scan from the test. The "toenail" shaped crack front is not seen in the simulation. The fact that the force displacement matches well but the facesheet damage does not agrees with the observation from Section 4.2 where facesheet cracking was found to be responsible for a small amount of energy dissipation when compared to the core crushing.

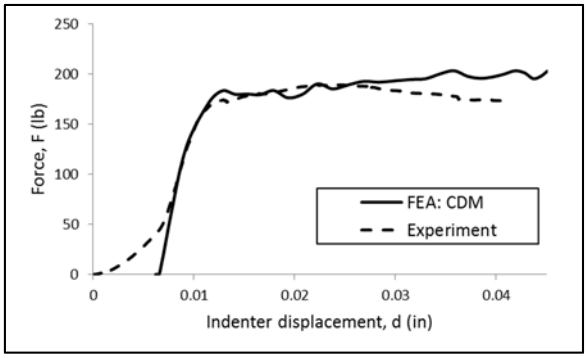


Figure 18. CDM: force displacement data correlation.

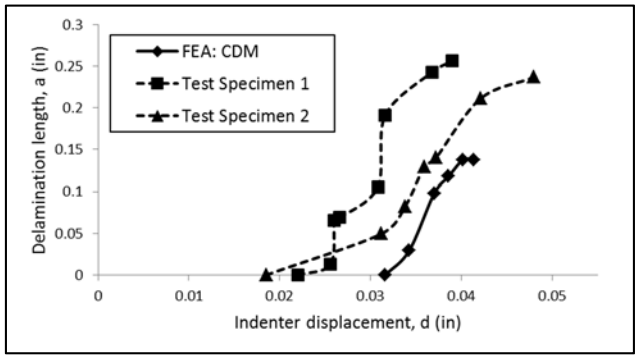


Figure 19. CDM: delamination length data correlation.

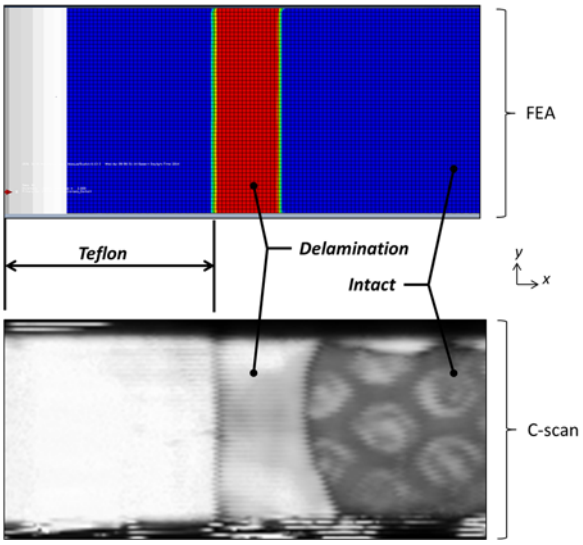


Figure 20. CDM: delamination front data correlation (plan view of specimen).

The poor agreement between the model and the experiment in facesheet damage is likely associated with the way that the Hashin/continuum damage formulation for composites is implemented in ABAQUS/Explicit® 6.13. This damage modeling tool is implemented for planar type elements only and therefore is intended for use in the traditional "1-2" plane of a composite plate. It does not contain transverse stress terms in the initiation or element stiffness degradation formulations. As a result, for this problem, damage initiation is delayed and a fully damaged element still retains the ability to carry a transverse shear load. A three dimensional implementation of the continuum damage formulation for composites would likely make it a more appropriate tool for this problem.

## 5. Conclusions

An experiment has been conducted where a simple and repeatable damage process in the facesheet of a composite honeycomb specimen was created. Facesheet damage, starting with an initial delamination, consisted of an intralaminar matrix crack followed by a delamination. This sequence of events was intended to be a simple damage process that could be understood well and therefore used as a means to evaluate the performance of numerical damage simulation tools. Under quasi-static indentation, the honeycomb core crushing is responsible for dissipation of the majority of the energy from external work. This serves to stabilize the damage process in the facesheet and allows it to be characterized in high detail.

A three dimensional finite element model of the composite honeycomb specimen was created to evaluate the ability of existing numerical tools currently implemented in ABAQUS/Explicit® 6.13. Much of this effort went into understanding the core crushing behavior as an isolated damage process and the subsequent verification of this aspect of the finite element models. The simulation agrees very well with experimental data for a pristine specimen where an initial delamination was not present. The verification and validation of this model was critical to subsequent analyses as the core crushing determines the deformed shape

of the facesheet and therefore strongly influences any damage process that occurs there.

When an initial delamination is included in the facesheet, both the CDM and CZM are capable of simulating the correct damage process. In this case, the CZM is more accurate, however. The CZM underpredicts the final delamination crack length by approximately 8% whereas the CDM underpredicts it by 47%. Also, the delamination initiation is delayed significantly in the CDM.

The CZM, while better simulating the damage process, is not necessarily a practical tool that can be widely applied to a variety of problems. The damage evolution path is prescribed *a priori* so it cannot be used in any predictive capacity. The CDM overcomes this limitation by allowing the migration to form anywhere in the mesh that a continuum damage material is defined. If the Hashin and continuum damage formulation implementation was enhanced in ABAQUS/Explicit® 6.13 to be fully three dimensional and include transverse stress components, it would likely be a more accurate and applicable tool for this problem.

## REFERENCES


1. Rose, C., C. Davila, F. Leone. 2013. "Analysis Methods for Progressive Damage of Composite Structures," NASA /TM-2013-218024.
2. Turon, A., C.G. Davila, P.P. Camanho. 2007. "An engineering solution for mesh size effects in the simulation of delamination using cohesive zone models," *Engineering Fracture Mechanics,* (74)10:1665-1682.
3. Rybicki, E.F., M.F. Kanninen. 1977. "A finite element calculation of stress intensity factors by a modified crack closure integral," *Engineering Fracture Mechanics* (9)4: 931-938.
4. Irwin, G.R. 1958. Fracture I, *Handbuch der Physik VI,* Flugge (ed), Springer Verlag, Berlin, Germany, 558-590.
5. Krueger R. 2004. "Virtual crack closure technique: History, approach, and applications," *Applied Mechanics Review*, (57)2:109-143.
6. Moes, N., J. Dolbow, T. Belytschko. 1999. "A finite element method for crack growth without remeshing," *International Journal for Numerical Methods in Engineering*, (46)1:131-150.
7. Matzenmiller, A., J. Lubliner, R.L. Taylor. 1995. "A constitutive model for anisotropic damage in fiber-composites," *Mechanics of Materials*, (20)2:125-152.
8. Hallett, S.R., B.G. Green, W.G. Jiang, M.R. Wisnom. 2009. "An experimental and numerical investigation into the damage mechanisms in notched composites," *Composites Part A: Applied Science and Manufacturing*, (40)5:613-624.
9. Pernice, F., L. Kawashita, S. Hallett. 2011. "An investigation of delamination and matrix crack interaction in mode-I failure of angle-ply composites using a cohesive zone model," University of Bristol Project, Bristol, UK.
10. Greenhalgh, E.S., C. Rogers, P. Robinson. 2009. "Fractographic observations on delamination growth and the subsequent migration through the laminate," *Composites Science and Technology*, 69(14):2345-2351.
11. Canturri, C., E.S. Greenhalgh, S.T. Pinho, J. Ankersen. 2013. "Delamination growth directionality and the subsequent migration process – The key to damage tolerant design," *Composites Part A: Applied Science and Manufacturing*, (54):79-87.
12. Ratcliffe, J.G., M.W. Czabaj, T.K. O'Brien. 2013. "A Test for Characterizing Delamination Migration in Carbon/Epoxy Tape Laminates," NASA TM-2013-218028.
13. Ratcliffe, J., W.C. Jackson, J. Schaff. 2004. "Compression strength prediction of impact-damaged composite sandwich panels," Proceedings of the American Helicopter Society 60th Annual Forum, Baltimore, MD.
14. Czabaj M. 2014. Private communication, NASA Langley Research Center, Hampton, VA.
15. Dassault Systems. April 2, 2013. Abaqus 6.13 Analysis User Manual.

16. Sjoblom, P.O., J.T. Hartness. 1988. “On low velocity impact testing of composite materials,” *Journal of Composite Materials*, (22)1:30-52.
17. Jackson, W.C., C.C. Poe Jr. 1993. “The use of impact force as a scale parameter for the impact response of composite laminates,” *Journal of Composites Technology & Research,*15(4):282-292.
18. Choi, I.H., C.S. Hong. 1994. “New approach for simple prediction of impact force history on composite laminates,” *American Institute of Aeronautics and Astronautics*, (32)10:2067-2072.
19. Correlated Solutions. 2010. “Vic-3d Reference Manual.”
20. Camanho, P.P., P. Maimi, C.G. Davila. 2007. “Prediction of Size Effects in Notched Laminates Using Continuum Damage Mechanics,” *Composites Science and Technology*, (67)13:2715-2727.
21. http://www.matweb.com, MatWeb©, Material Property Data, Aluminum 5052-H38.
22. Benzeggagh, M.L., M. Kenane. 1996. “Measurement of Mixed-Mode Delamination Fracture Toughness of Unidirectional Glass/Epoxy Composites with Mixed-Mode Bending Apparatus,” *Composites Science and Technology*, 56(4):439-449.
23. Lapczyk, I., J.A. Hutado. 2007. “Progressive damage modeling in fiber-reinforced materials,” *Composites Part A: Applied Science and Manufacturing,* (38) 11:2333-2341.